Application of dynamic thermal rating: Overhead line critical spans identification under weather dependent optimized sensor placement

Saifal Talpur*, T. T. Lie, R. Zamora

School of Engineering, Computer and Mathematical Sciences, Auckland University of Technology, New Zealand
*Corresponding author email: saifal.talpur@aut.ac.nz

Abstract

Dynamic thermal rating (DTR) for an overhead transmission line is a viable and cost-effective technique based on real weather conditions to mitigate congestion and avoid load shedding for reliable transfer of the required electricity. Spans of overhead lines passing through multiple geographical regions face diverse weather conditions and varying terrain, and thus need to be monitored to obtain reliable estimates of line loadability. Spans facing the worst weather and with the longest length determine the absolute minimum line loadability and are therefore known as critical spans. Identifying critical spans is important in allowing utility providers to monitor their overhead transmission networks spanning large geographical regions. This paper focuses on identifying critical spans using the proposed technique to find the bottleneck to the overhead transmission network for optimum power transfer. It determines the optimal number and placement of sensors across the entire test line, dividing the line into non-uniform segments, each carrying multiple length spans passing through flat and non-flat terrains. The resulting critical spans determine the line loadability that can effectively relieve transmission line congestion, based on the allowable vertical clearance to the ground. The outcome of the proposed technique is validated against the conventional technique for critical span identification.

Keywords: *Dynamic thermal rating, critical line spans, optimal sensor placement, non-uniform line segmentation, weather conditions and span topography, line congestion and load shed management*

1. Introduction

To meet the growing demand for electricity, overhead transmission lines are required to transfer additional electricity with no ground clearance infringements. The capacity of overhead transmission lines is determined by their physical dimensions, surrounding weather conditions, maximum allowable temperature and the allowable distance from the ground. An overhead line passes through multiple geographical regions, where each span faces considerably different weather conditions.

As each span of an overhead line differs in length, weather conditions and route, the span elongation across each line span varies depending on space and time, even under the same loading and operational conditions. Therefore, the dynamic thermal rating (DTR) for the entire line cannot be calculated by ignoring the individual span lengths and their surrounding weather conditions as these may cause adverse sagging across spans facing the worst weather conditions during the loading period. The spans with minimum clearance to the ground at specific loading condition are called critical spans.

Critical spans operate at the highest temperature with the lowest current-carrying capability in a tensioning section between two towers. The span topography and ambient conditions across a line span are critical in its ability to transfer the required electricity. Because of the time- and space-dependent weather conditions affecting an overhead line, critical spans do not remain fixed or static; they rather vary over the entire length. Critical spans with the longest length passing across valleys, river-crossings, highways and varying terrains, face comparatively the worst real-time weather. The critical spans in an overhead line cause hot-spot temperature, which is a primary variable for determining the line loadability. Thermal line ratings based on hot-spot temperatures provide reliable thermal-limit estimates in comparison to

computing the thermal line rating based on an overall estimate of weather elements across an overhead line with no consideration of critical spans.

A critical line span is a span exposed to the worst weather elements, of the longest length, passing over varying terrains. Critical spans play an important role in solving the optimal power flow problem in terms of considering the thermal constraints across the entire line-length. The location and corresponding line temperatures across critical spans are very important for system operators in dynamically assessing the line hot-spot temperatures and thus finding reliable line loadabilities, as investigated in this paper. Critical span identification will help utilities to decide when and how much load an overhead transmission line can safely carry. Critical spans experience comparatively higher hot-spot temperatures at the same thermal loadability to non-critical line spans. Therefore, this paper focuses on identifying these spans to determine a reliable line-loadability within allowable sag limits.

The proposed technique validates the concepts as presented in [1]-[2], that the critical span is not a fixed span; rather it varies with space and time. The proposed technique thus suggests an optimum number and placement of sensors across the entire line. Instead of placing sensors across some assumed or non-validated critical spans, the proposed technique will find the optimum sensor placements for monitoring of time- and space-dependent weather across each line span. To address the spatial variability in ambient conditions, the entire test line in this paper was monitored to give a reliable estimate of weather-dependent critical spans. The line was therefore divided into multiple segments from the sending to the receiving ends.

Due to involving the optimized segment locations, this segmentation approach will have less computational burden compared to the segmentation technique in [3]

and [4], where each line span is considered as a segment. This study broadened the segmentation approach used in [3]-[4], which segmented a large overhead line based on ambient temperature differences but ignored the span length effect and weather influences on span sagging levels. The segmented approach in this paper addresses both system-level studies and detailed component modeling, advancing the line-segmentation approach in [3]-[4], which focuses on system-level studies rather than detailed component modeling.

Critical span identification in a DTR-operated overhead line was carried out in [5] to determine the line sagging limits in comparison to the approach presented in [6]. The critical span identification technique in [5] focuses on identifying the critical spans based on correlation benchmarks between minimum line ratings derived from initially assumed line critical spans, giving the global minimum of the line thermal capacity, and the line thermal capacity derived from all line spans. A higher correlation benchmark between both ratings is the decisive factor in considering the span as critical. The technique has a limited scope as it requires knowledge of one critical span in order to identify the other critical spans. The critical span identification technique presented in [5] is similar to the identification technique in [6].

Because the technique ignores the span-topography and terrain levels in critical span identification, the derived sagging levels in [5] may be different to those determined by considering span topography and terrain variability. The sag across critical spans will therefore result in unreliable estimations of distance from the ground. The algorithm also does not consider the critical span sagging during static weather conditions and considers line loading above the maximum allowable temperature (MAT) limit, which may result in excessive sag, reduced tensile strength and increased conductor aging.

Additionally, in [6] the distance between segments is chosen without consideration of optimal sensor placements. The drawback of this random selection can be in terms of weather estimation data across each segment and hence across each line span between segments, resulting in unreliable line thermal ratings. The critical span identification technique as presented in [6] requires a set of monitoring stations to achieve the required confidence level. It means, in case of non-availability of the required set of weather stations, monitoring of a selected set of spans, rather than every line span across the entire line, can be done. Also, to find the correlation-based confidence level between thermal capacity across each span and thermal capacity across the whole line, the algorithm will impose a huge computational cost for critical span identification. Additionally, as the algorithm does not consider the effect of dynamic thermal ratings on span sagging levels, the estimated thermal rating for the whole line may result in excessive sagging levels, particularly across the identified critical spans.

Multiple critical spans exist across a single overhead line. Hence, identifying the factors that influence the location and number of critical spans is crucial for utility providers [7]. This paper refines the methods proposed in [5]-[7] to identify critical line spans based on varying terrain levels not addressed in [5] and sag modelling not considered in [6] and [7]. Location of critical spans across any overhead line requires knowledge about weather elements and the span topography, the factors that were ignored in [8] and [9] while determining the critical spans. The installation of weather monitoring sensors across every span of an overhead line passing through a vast geographical region would require a huge capital investment.

In order to achieve the required accuracy across each line span at a reduced cost, this paper introduces a novel method to provide weather data across every

span of an overhead line passing through a large geographical region while facing multiple weather patterns across varying terrains. The proposed technique enhances transmission planning and sensor installment by determining the optimal number and location of sensors across each segment in the test overhead line to locate critical spans during the entire operation of the test line.

The proposed technique in this paper fills the gap identified in [1]-[9] by considering the weather and span topography individually across each span in all line segments of the test overhead line, giving a reliable estimation of critical spans or the bottlenecks. The proposed technique provides optimal number and location for sensor installation to identify critical spans across the test overhead line. Thermal line ratings based on the identified critical spans result in line flow with no ground clearance infringements. In addition to critical sag monitoring during dynamic weather conditions, the presented approach also considers span sagging levels during static weather conditions.

The research gap summary over literature [1]-[9] along with contribution of this study is shown in Table 1. To fill the research gap illustrated in [1]-[9], this paper presents a unique methodology:

i. To determine the optimal number and placement of sensors using a supervised sensor placement approach.
ii. To identify the critical line spans using weather and span length considerations to produce no ground clearance infringements in any line span.
iii. To determine the temperature and sagging level across all line spans and across the identified critical spans to find the minimum line thermal rating capacity during both static and dynamic weather conditions.

Table 1 Literature, research gap and contributions summary

Research gap from the literature	Contributions of the study
The study in [1]-[2] considered identification of spans with highest temperature or minimum loadability without taking into account the span topography information along with weather elements across each line span.	An optimization algorithm is developed to find the minimum optimum number and sensor placements for considering the ambient conditions across the entire test line including short distances and remote locations to find temperature and sag across each line span based on span topography and ambient data available from a few weather stations.
In [3]-[4], a non-uniform line segmentation approach was carried out with following unaddressed issues: • Number and placement of segments was determined through variation in ambient temperature from the threshold. • Ambient temperature was the only weather parameter considered in terms of determining the line temperature between and across the segments.	In the developed algorithm, line segmentation is carried out under system and component level modelling to further assist in the identification of weather and topography based critical spans with following contributions over [3] and [4]. • An optimized sensor numbering, and placement based on location of reference weather stations between the line sending end to the line receiving end was obtained. • The resulting line segments were used to determine the weather across and between each line segment in the entire line length.
The approach presented in [5]-[6] for critical span identification have left following gaps: • Critical spans are identified without considering the span topography and the type of terrains. • The process to identify critical spans requires knowledge about the span with smallest ground clearance or minimum thermal loadability in advance. • The techniques are presented under steady-state thermal line modelling that mainly identify time and space independent critical spans under thermal equilibrium state due to considering the constant weather and loading conditions.	The proposed design algorithm fills the gap from [5]-[6] with following contributions: • Critical span identification technique considers span topography and the rugged terrains (mainly the case in New Zealand) besides span weather conditions to accurately determine the number and placement of time and space dependent critical spans during each loading time interval. • The proposed technique does not require in advance the knowledge of span with minimum thermal loadability. • Non-steady state modelling under realistic loading scenarios is considered to validate accuracy and computational efficiency of the proposed algorithm under time-space dependent ambient, time dependent loading and space dependent terrain conditions.
The gaps and contributions from [7]-[9] are: • The testing was carried out on a single test span under steady-state heat-balance [7]. • In [8], an optimized sensor placement technique was designed without considering the span sag-temperature relationship. The study presented in [9] examined sagging across inclined spans and provided the detailed mathematical modelling.	A detailed mathematical modelling approach is employed in this paper under non-steady state heat balance after addressing the following gaps from [7]-[9]: • The designed algorithm has considered weather, span topography and type of terrains across all line spans before deciding the hot spots. • The presented study provided the proof of concept validation with conventional critical span technique and is found reliable. • The study has addressed sagging across both levelled and inclined spans while passing through flat and non-flat terrains respectively.

By considering both geo-spatial weather and temporal loading conditions towards affecting the sag across each span of the test line, the proposed critical span identification technique provides a true representation of the maximum thermal capacity limit of the line. The proposed technique provides an effective solution for computing thermal line ratings using real-weather conditions, where utility companies, due to non-availability or difficulty in measuring or estimating the real weather conditions across every span of an overhead line, are currently obliged to use static thermal line ratings based on conservative assumptions that ignore fluctuating time- and space-dependent weather conditions.

The proposed technique besides involving less computational burden is a viable solution for utility companies for determining the thermal capacity of their overhead assets effectively and reliably under no ground clearance violations during the excess electricity transfer. Critical spans identified under both the conventional and the proposed technique are compared to examine the reliability and computational efficiency of the proposed technique.

The rest of the paper is structured as follows: Section 2 highlights thermal line rating and discusses the test system and weather modelling. Section 3 presents the design methodology of the proposed and conventional critical span identification techniques. Section 4 presents the case study. Section 5 provides the obtained results. Section 6 summarizes the findings of the paper.

2. Line Model

2.1. Non-steady state electro-thermal line modelling

Overhead lines are rated statically and dynamically. In both conditions, the conductor rating is calculated using the heat balance between heat gain and heat loss via the heat balance equation (HBE) under steady and non-steady state

conditions. In this paper, HBE was considered under non-steady system state, where, electro-thermally coupled (ETC) line modeling [10] was examined. The purpose of utilizing the ETC technique was to increase the line utilization and in result remove line congestion and possible load-shedding, further demonstrated in [10]. The HBE under dynamic or non-steady state conditions as shown in (1) consists of heat absorption and heat emission [11]. Heat absorption takes place due to load-dependent flow of current in the core and the surface of the conductor ($\boldsymbol{I_s^2(t)}$) and due to the ability of the conductor to absorb time varying solar radiations $\boldsymbol{P_s^s(t)}$. Heat emission is the phenomenon that takes place due to heat convection ($\boldsymbol{Q_s^c(t)}$) and heat radiation ($\boldsymbol{Q_s^r(t)}$) from the overhead conductor [12]-[13] as shown in (1).

$$m * C\frac{dT_s(t)}{dt}\left(HBE(t)\right) = \left(\left(k_{ac} * R_{dc} * I_s^2(t) * T_s(t)\right) + \left(P_s^s(t)\right) - \left(Q_s^c(t)\right) + \left(Q_s^r(t)\right)\right) \quad (1)$$

where $\boldsymbol{m}$ is the conductor mass, $\boldsymbol{C}$ is the conductor's specific heat capacity measured as the ratio between the conductor's heat capacity and its mass in J/kg·°K, $\boldsymbol{P_s}$ $\boldsymbol{(t)}$ represents solar heat gain, $\boldsymbol{Q_c(t)}$ and $\boldsymbol{Q_r(t)}$ represent convective and radiative cooling, respectively. $\boldsymbol{I_s(t)}$ is the time and line loading-dependent flow of current through span $\boldsymbol{s}$, and $\boldsymbol{T_s(t)}$ is the space- and time-dependent span temperature.

The HBE under steady and non-steady system states acts differently, i.e., under steady or constant system states, the sum of heat absorption and heat conduction is always identical causing the overhead line under thermal equilibrium state. Contrary to that, under changing ambient and loading conditions, the difference between heat absorption and heat conduction becomes greater than zero leading to thermal inequilibrium state as studied in [10]. This additional energy due to involving thermal inertia causes thermal instability in the overhead line, further dependent on conductor's mass and specific heat capacity. In this paper, HBE under non-steady

thermal state is considered due to a linear relationship between span length, conductor mass and thermal inertia that is further needed when identifying the line spans with minimum thermal loadability and critical sagging. Additionally, the line thermal rating technique under non-steady state can be used to accurately determine the maximum optimal capacity of the overhead line and the time it can stay overloaded and thereby allowed optimum power flow under safe allowable conductor temperature limit.

In this paper, the test line is loaded from a lower $\boldsymbol{I_1(t)}$ loading current to a higher loading current $\boldsymbol{I_2(t)}$ current causing conductor in heating state $\boldsymbol{C_h^{max}(t)}$ as described in (2) [10] and from a higher $\boldsymbol{I_2(t)}$ to a lower $\boldsymbol{I_1(t)}$ loading current making conductor under the cooling state $\boldsymbol{C_c^{min}(t)}$ as described in (3) [10]. The cycle is continued until the test overhead line reaches its MAT limit $\boldsymbol{T_c^{max}(t)}$.

$$C_h^{max}(t) = \frac{(I_2^2(t) * R_{ac}(t)) + (P_s(t))}{\pi * D * (T_c^{max}(t) - T_a(t))} \quad (2)$$

From (3), it is evident that higher conductor diameter $\boldsymbol{D}$ and lower ambient temperature $\boldsymbol{T_a(t)}$ reduce conductor heating and allows more current to flow at lower series AC resistance $\boldsymbol{R_{ac}(t)}$.

$$C_c^{min}(t) = \frac{(I_1^2(t) * R_{ac}(t)) + (P_s(t))}{\pi * D * (T_c^{min}(t) - T_a(t))} \quad (3)$$

2.2. Test system modelling

To testify and validate the proposed algorithm on realistic case scenarios, a realistic test system resembling the New Zealand's north island transmission network (as shown in Fig. 1) was modeled in DIgSILENT®. The modelled power system involved two parallel overhead lines connected between Huntly power station and the Penrose substation, situated in New Zealand's north island transmission network

as shown in Fig. 2. Physical dimensions of both overhead lines as taken from [14] are provided in Table 2, where Line-1, referred to as the test overhead line throughout this paper, is a Grape aluminium conductor steel reinforced (ACSR), 86 km in length with an operating voltage of 132 kV. The modeled system in Fig. 2 is referred as the test system throughout this paper.

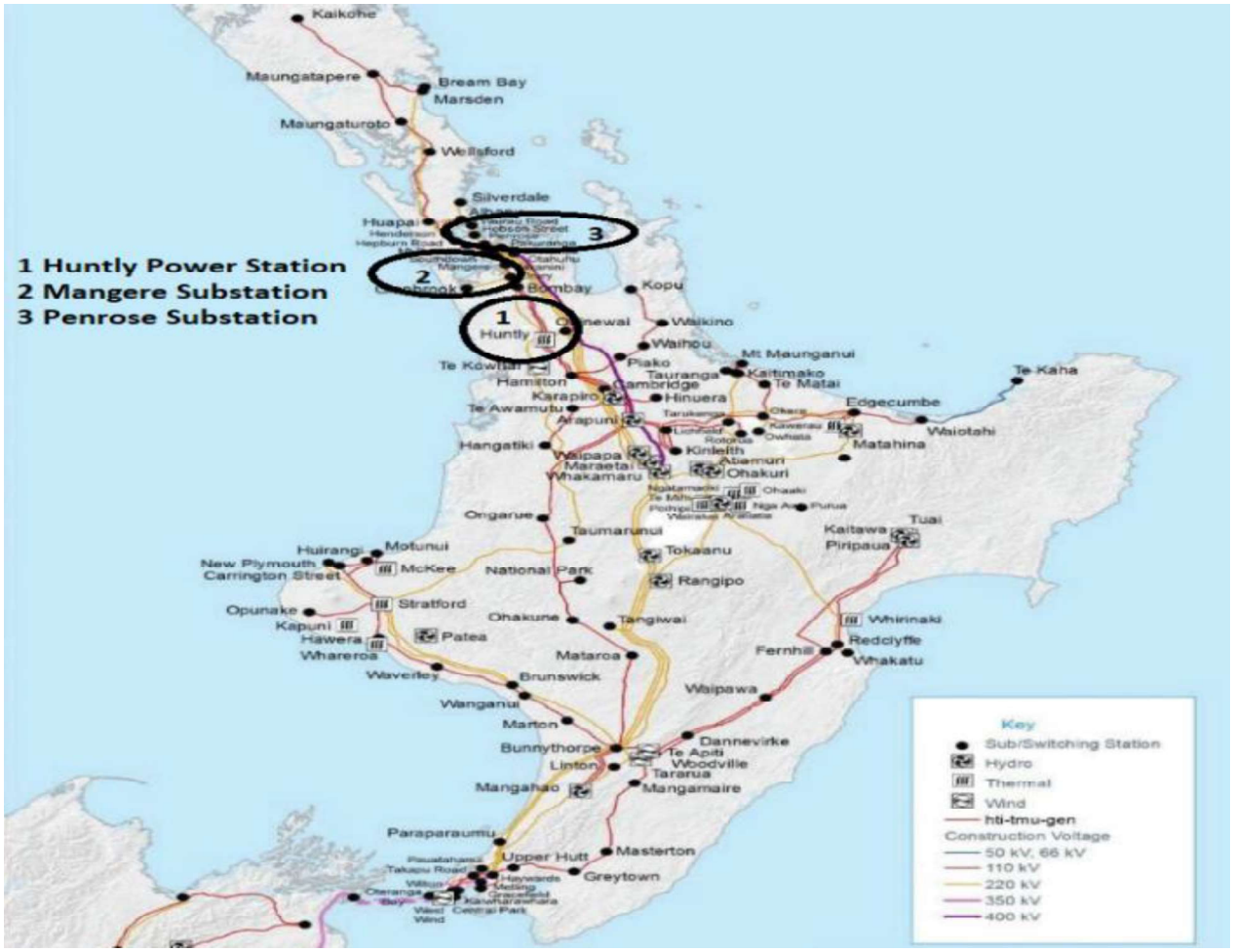

Fig. 1 Transpower's north island transmission network in New Zealand

The test overhead line was assumed to have multiple segments and each segment had $\boldsymbol{n}$ number of non-equidistant spans. The 10-min interval-based ambient data consisting of ambient temperature, wind speed and solar radiation on a hottest day in January-2019 was collected from [15] and filtered to 5-min intervals from reference weather stations across the route of the subject overhead line as shown in Table 3. The day selection was based on finding the worst real weather conditions.

Table 2 Line physical dimensions

Overhead Lines	Diameter (mm)	Conductor Mass (kg/m)	Coefficient of linear expansion x10^{-6}/°C
Line-1	17.5	0.677	19.4
Line-2	31.5	1.96	20.6

Table 3 Line segmentation

Segment	Reference weather stations	Total Number of spans	Spans near weather stations
Huntly-Mangere	Pukekohe & Mangere	457	2
Mangere-Penrose	Owairaka	60	1

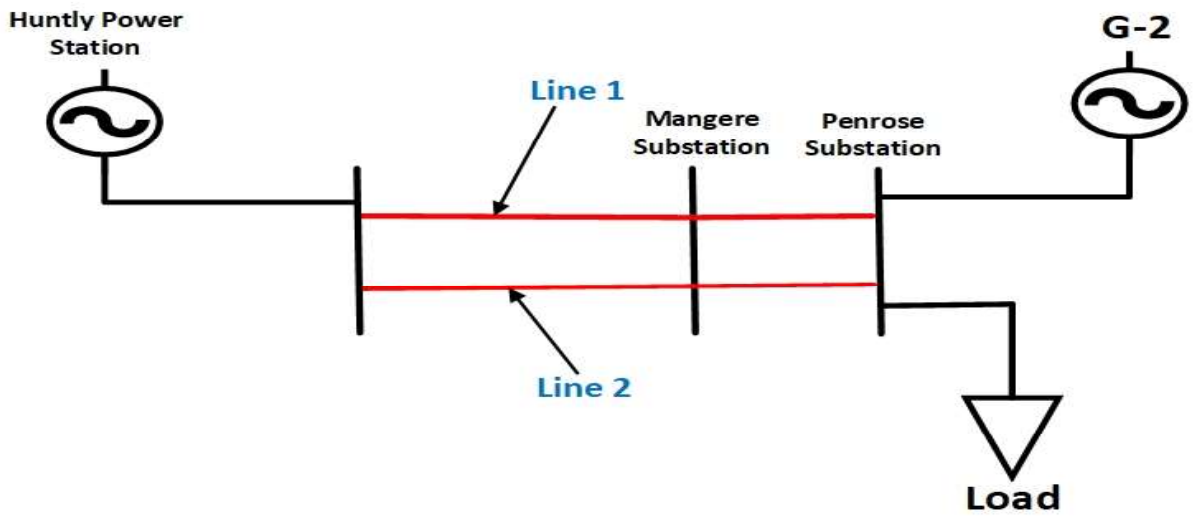

Fig. 2 Single line diagram of modelled test system

For the sag modeling, the test overhead line was considered to be a semi-urban type with 12% ultimate tensile strength (UTS) [14]. Further shown in Fig. 2 and Table 3, the test overhead line sending-end at Huntly power station has a nearby weather station at Pukekohe. Similarly, the receiving-end of the test line at Penrose substation has a nearby weather station at Owairaka. The test overhead line was assumed to run between Huntly power station and the Penrose substation with

reference weather stations at Pukekohe, Mangere and Owairaka with total number of spans as shown in Table 3.

The line was divided into multiple segments from the line sending-end to the line receiving-end, with each segment containing multiple spans with real weather data obtained from 3 weather stations [15]. The length of these spans varied between 80 m and 240 m and were taken from [14], where the longest line spans were assumed to pass through varying terrain. The test overhead line spanning over three weather stations with each weather station representing a single line span (the line between two towers).

In the test system, the cost-effective and fast-responsive based re-dispatchable electricity generation at Huntly power station was transferred to the load through test line and Line-2. At the time when Line-2 was disconnected for temporary maintenance, the most feasible option to avoid load shedding was to pass excess electricity through the test line under the DTR technique in place of costlier and slow-responsive generation dispatch from G-2. To mitigate possible congestion (due to N-1 state), the test line was operated under the DTR technique. The test overhead line was loaded based on two practical case scenarios where the line's thermal capacity was checked during the dynamic state of the modelled power system. The line current from the test system was fed into the line thermal capacity algorithm to find the maximum thermal capacity of the test line under the constraints of minimum allowable ground clearance of the critical spans and the line's MAT limit (set at 80°C).

2.3. Weather modelling

Due to the limited weather stations near the test overhead line, the weather data across spans distant from the weather stations were derived from the weather data

across spans near to the reference weather stations, as shown in Table 3, using a piece-wise linear regression technique [16]. The purpose of using this technique is twofold: 1) it needs few inputs to give the desired outputs and 2) the resulting outputs meet the set threshold criteria and therefore the estimated unknown parameters fall within the specified data range.

The derived weather data across spans at each segment-start and segment-end (represented as optimal sensor locations, further described in section 3.1) were then used to find the unknown weather data for each span in the test line. In (4), parameters related to the known weather data are given as the inputs, while the estimated value of weather elements across every span in each segment of the test overhead line is the output.

$$E(Y|X) = \left(\alpha * (Y_{min}, X_{min})\right) + \left(\sum_{s=2}^{N} (X_s * \beta_s) * |(Y_{max}, X_{max}) - (Y_{min}, X_{min})|\right) \quad (4)$$

where $\boldsymbol{E(Y|X)}$ is the estimated value of dynamic weather elements $(\boldsymbol{T_N^a(t)}, \boldsymbol{V_N^s(t)}, \boldsymbol{Q_N^s(t)})$ across all the line spans in one segment of the test line, from the segment-start to the segment-end with respect to span lengths in the whole segment. $\boldsymbol{\alpha}$ is the intercept co-efficient. $\boldsymbol{Y_{min}}$ is the minimum value of weather elements in a segment. $\boldsymbol{X_{min}}$ is the minimum segment distance from the line sending-end. $\boldsymbol{X_s}$ is the distance from the first reference weather check-point of the segment to the next consecutive span of the segment. $\boldsymbol{\beta_s}$ is the slope parameter of spans $(\boldsymbol{2 \leq s \leq N})$ in every segment of the test line. $\boldsymbol{Y_{max}}$ is the maximum value of weather elements in a segment. $\boldsymbol{X_{max}}$ is the maximum segment distance from the line sending-end and $\boldsymbol{N}$ is the total number of spans in the entire segment. The same procedure is then used for all segments in the test line.

3. Critical span identification algorithms

3.1. Proposed algorithm design overview

To identify critical spans in the test overhead line, it is considered that any long overhead line passing through several geographical regions will face multiple weather conditions due to changes in altitude, wind pressure and terrain topography [3]. The flow-chart in Fig. 3 presents the proposed methodology to identify multiple critical spans across the entire line, operating under both static and dynamic line rating techniques. Fig. 3 further illustrates segmenting the test line to identify the critical spans through mathematical modelling, described in Step 1 through Step 3 and in Algorithm 1 through Algorithms 2(a) and 2(b). After critical span identification, sag-modelling was carried out in Step 4.

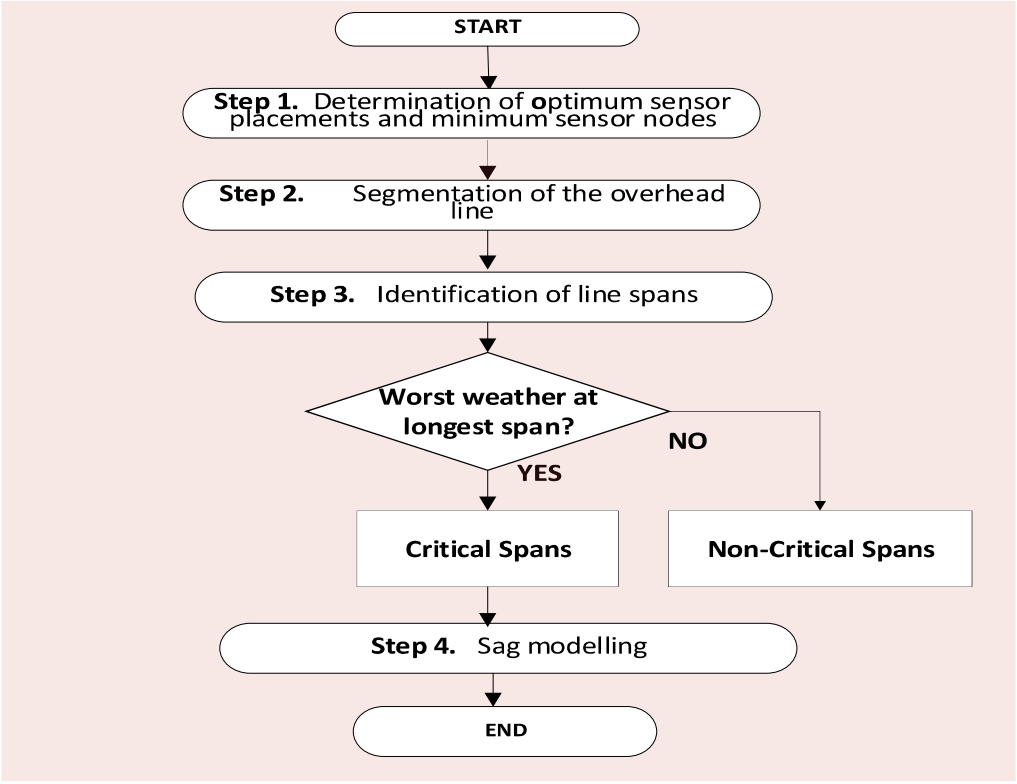

Fig. 3 Simplified flow-chart for proposed critical span identification

Step 1) Optimal Sensor Placement

The optimal number and placement of sensor nodes across the test overhead line was determined from the line sending-end to the line receiving-end. The sensor

placement was carried out in such a way that weather data across every line segment was required to estimate the weather conditions in every line span.

In the calculation, i represents sensor node placement, where 1 represents optimal sensor placement and 0 represents non-optimal sensor placement. $\boldsymbol{l}$ is the length of the test line, 86km in this case. To determine the minimum number and optimal placement of the sensor nodes, the sparse-aware sensor selection (SparSenSe) technique [17]-[18] was used, as discussed in (5)-(8).

$$w_i \in \{0,1\}, i \in \|l\| \tag{5}$$

When the i^{th} variable of the selection vector $\boldsymbol{w}$ is 1, the sensor placement is optimal, and its corresponding measurement is used over $\boldsymbol{l}$. As shown in (6), the first variable of the selection vector represents the sending-end of the line while the last variable represents the receiving-end of the test overhead line.

$$w = \left[w_{BEG,1}, \cdots, w_{END,M}\right]^T \tag{6}$$

Similarly, the size of the vector $\boldsymbol{u}$, representing the line segments as shown in (7), is greater than the size of the selection vector $\boldsymbol{w}$ in (6). This means the calculated sensor measurement nodes $\boldsymbol{M}$ will be lower than the total number of segments $\boldsymbol{n}$ due to the lack of sensor placement across segment-ends near the weather stations over the line length $\boldsymbol{l}$. This condition is further discussed in Step 2.

$$u = [u_1, \cdots, u_n]^T, \quad M < n \tag{7}$$

The minimum optimization problem in (8) is solved by keeping the mean square error (MSE) below the threshold $\boldsymbol{\gamma}$ of 1%.

$$\begin{aligned} &(\hat{w}, \hat{u}) := \arg\ min\ \{\|w\|_1\} \\ &w \in [0,1]^M, u \\ &\text{s.t.} \quad \{(w,u) \in (0 \le \gamma \ll 1)\} \end{aligned} \tag{8}$$

Equations (5)-(8) represent a linear inequalities problem and are therefore solved using a MATLAB-based convex optimization (CVX) toolbox [19]. Steps to find the

optimal sensor numbers and placements, as shown in Algorithm 1, use the total line length and reference node locations from the nearby weather stations as the reference distances to initialize the optimum sensor placement technique.

Algorithm-1: minimum sensor number & optimal placements

Input: Set $w_i^* > \gamma, \text{where } 0 \leq \gamma \ll 1$, to get $w_i^* \neq 0$

***Step-1*:** Determine the optimum sensor placements

for $w_i^* \neq 0$

$w_i^* > \gamma$

optimum sensor placement = SparSenSe [($\hat{u}$, γ)]

end

***Step-2*:** Determine the required minimum sensor nodes

for optimum sensor number = $(w_{BEG,1}: 1: w_{END,M})$

MSE = optimum sensor placement {(1: n), $\hat{u}$}

end

Output: $\mathrm{w}_i^* = [(\hat{u}, \text{MSE})]$

Step 2) Line Segmentation

The purpose of line segmentation is to find the individual weather conditions across each span of the test overhead line. Due to the limited number of available weather stations from the line-sending end to the line-receiving end, weather elements across spans near the weather stations were taken as reference values for estimating the unknown weather elements across the rest of the segment-ends, as mentioned in Step 2.3. The estimated weather data across each segment-end were used to find the unknown weather data at every span between two consecutive segments for the entire length of the test line. The proposed line segmentation approach is described in detail in Steps 2.1-2.3.

Step 2.1) Based on the Algorithm 1 output, optimum sensor-placement was carried out over the entire test line. The resulting sensor placement was found to

divide the line into 50 non-equidistant segments, where each segment carried one tensioning section $\boldsymbol{\varphi}$. The minimum distance between two consecutive tensioning sections from the SparSenSe technique was found to be 1 km at 18 locations, and the maximum distance obtained was 7 km at one location. As shown in (9), each segment along a line of length $\boldsymbol{x}$ consists of a tensioning section $\boldsymbol{\varphi}$ with $\boldsymbol{s}$ spans ranging between 80 m to 240 m in length. The resulting non-equidistant spans were arranged by shuffling the array of span elements in MATLAB®.

$$x_{seg}^{\varphi_1,\cdots,\varphi_n} \equiv \left[x_s^{\varphi_1},\ \ x_s^{\varphi_2}\ ,\ \ \cdots\ \ x_s^{\varphi_n}\right]^T,\ s = 1, 2, \cdots, N \tag{9}$$

The division of $\boldsymbol{x_{seg}^{\varphi_{1,2,\cdots,n}}}$ segments as shown in (9) was based on an optimal number of sensor placements; i.e., a segment was proposed between two sensor nodes, where each end of the segment is considered as a weather check-point. Thereafter, each individual segment was observed to carry $\boldsymbol{N}$ number of spans ranging between 80 m and 240 m in length. The strategy followed in creating the line segments is further explained in Step 2.2.

Step 2.2) As shown in (10), the known weather elements across spans near the reference weather stations in Table 3 were used to find the unknown weather elements at the segments across weather check-points using the linear piece-wise regression technique [16, 20] as shown in (4).

$$\begin{aligned} x_k^R&:\ [T^a(x_k), V^s(x_k), Q^s(x_k)\ ]^T \\ x_{k+1}^R&: [T^a(x_{k+1}), V^s(x_{k+1}), Q^s(x_{k+1})\ ]^T \\ x_{k+2}^R&: [T^a(x_{k+2}), V^s(x_{k+2}), Q^s(x_{k+2})\ ]^T \end{aligned} \tag{10}$$

In (10), $\boldsymbol{x_k^R}$ represents the set of weather elements at span $\boldsymbol{k}$ belonging to the first reference weather-station; similarly $\boldsymbol{x_{k+1}^R}$ represents the set of weather elements at

span $\boldsymbol{k+1}$, belonging to a second reference weather-station and $\boldsymbol{x_{k+2}^{R}}$ represents the set of weather elements at span $\boldsymbol{k+2}$, belonging to the third reference weather station.

Step 2.3) The known weather elements from Step 2.2 across each segment-end of the line were used to determine the unknown weather elements at every line span between each line segment, using the piece-wise regression technique [16, 20], where to maintain accuracy in the estimated weather elements, $\boldsymbol{\lambda}$ was limited to 0.1. As based on non-uniform span-lengths, each segment of the test overhead line was found non-uniformly distributed. Fig. 4 shows a non-uniformly distributed segment of the test line.

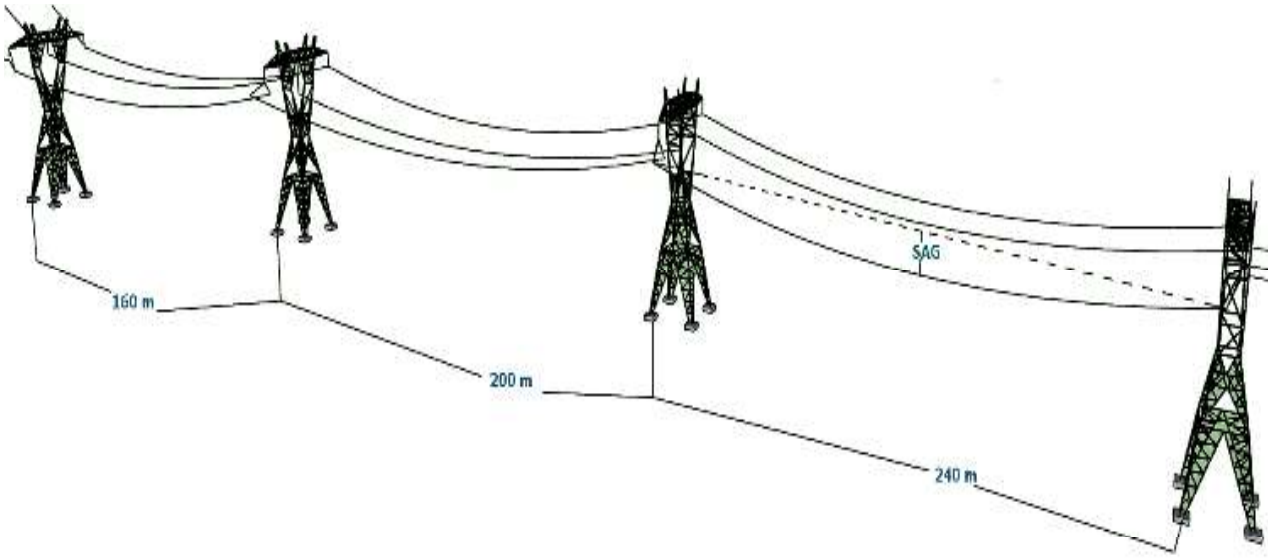

Fig. 4 Line sag modelling sketch in a tensioning section

Step 3) Critical Span Formulation

In this step, mathematical modelling of the proposed critical span identification technique was used to identify the set of critical line spans. The process of identifying the critical line spans in the test overhead line was carried out using the following sub-steps. This step was to identify the line spans passing through flat and

non-flat terrains that had the longest length and faced the highest ambient temperature, lowest wind speed and highest solar radiation, using the 'span length weather optimization problem' (SLWOP).

The optimization problem starts with the segmented line carrying $\boldsymbol{n}$ number of segments, where each line segment carries $\boldsymbol{N}$ number of spans with a total set of line spans $\boldsymbol{R_s}\left(\boldsymbol{x_{seg}^{\varphi_1,\cdots,\varphi_n}}\right)$ from the line sending-end to the receiving-end with a total set of multiple critical $\boldsymbol{R_c}\left(\boldsymbol{x_{seg}^{\varphi_1,\cdots,\varphi_n}}\right)$ spans and a total set of multiple non-critical line spans $\boldsymbol{R_o}\left(\boldsymbol{x_{seg}^{\varphi_1,\cdots,\varphi_n}}\right)$ as shown in (11).

$$R_s\left(x_{seg}^{\varphi_1,\cdots,\varphi_n}\right) = \left(R_c\left(x_{seg}^{\varphi_1,\cdots,\varphi_n}\right) + R_o\left(x_{seg}^{\varphi_1,\cdots,\varphi_n}\right)\right) \tag{11}$$

$\mathbf{SLWOP_1^{\varphi}}$ as shown in (12) elaborates the modelling procedure in selecting the critical line spans that face the highest ambient temperature in a dynamic-weather scenario. The procedure starts by searching for the maximum ambient temperature across all line spans lying across $\boldsymbol{n}$ segments of the test overhead line $\boldsymbol{x_1, \ldots, x_n}$ from the line sending-end to the line receiving-end, to identify the critical spans during loading time $\boldsymbol{t}$. The proposed formulation in (12) meets the condition that the obtained critical line span $\boldsymbol{c_{AB}}$ lying between towers $\boldsymbol{A}$ and $\boldsymbol{B}$ carries the longest length of all spans in the total set of line spans facing the maximum ambient temperature $\boldsymbol{T_{c_{AB}}^{a}}\left(\boldsymbol{x_{seg}^{\varphi_1,\cdots,\varphi_n}}\right)$.

$$\mathrm{SLWOP}_1^{\varphi}: \underbrace{max}_{\forall c_{AB} \in R_c \in R_s\left(x_{seg}^{\varphi_1,\cdots,\varphi_n}\right)} \sum_{s_1}^{s_N^{\varphi}} \left\{T_{c_{AB}}^{a}\left(x_{seg}^{\varphi_1,\cdots,\varphi_n}\right) \in T_s^{a}\left(x_{seg}^{\varphi_1,\cdots,\varphi_n}\right)\right\} \tag{12}$$

$$\text{s.t. } \beta_{s_1,\cdots,s_N}^{x_{seg}^{\varphi_1,\cdots,\varphi_n}} > \alpha_{c_{AB}}^{x_{seg}^{\varphi_1,\cdots,\varphi_n}} \geq max\left(L_{c_{AB}}\left(x_{seg}^{\varphi_1,\cdots,\varphi_n}\right)\right) \forall R_c \in R_s \in max\left\{T_{c_{AB}}^{a}\left(x_{seg}^{\varphi_1,\cdots,\varphi_n}\right) \wedge t, T_{c_{AB}}^{a}\left(x_{seg}^{\varphi_1,\cdots,\varphi_n}\right) \vee t\right\}$$

Based on the mathematical formulation of $\mathbf{SLWOP_1^{\varphi}}$, span $\boldsymbol{c_{AB}}$ is an identified critical line span lying between towers $\boldsymbol{A}$ and $\boldsymbol{B}$ in a segment that belongs to a set of multiple critical spans $\boldsymbol{R_c}$ that are a subset of the total line span set $\boldsymbol{R_s}$. Further,

$\mathbf{SLWOP_1^{\varphi}}$ is subject to the required sagging level, i.e., the calculated sag $\boldsymbol{\alpha}_{c_{AB}}^{x_{seg}^{\varphi_1,\cdots,\varphi_n}}$ across the identified critical span based on the DTR technique is less than the maximum allowable sag $\boldsymbol{\beta}_{s_1,\cdots,s_N}^{x_{seg}^{\varphi_1,\cdots,\varphi_n}}$ (see Section 5). To find another critical line span at the next loading time $\boldsymbol{t+1}$, $\mathbf{SLWOP_1^{\varphi}}$ is updated and the procedure is continued until all critical spans are identified.

Similarly, $\mathbf{SLWOP_2^{\varphi}}$ as shown in (13) elaborates the procedure in selecting the critical line spans facing the lowest wind speed in a dynamic-weather scenario. The procedure starts searching for the lowest wind speed across all $\boldsymbol{n}$ segments ($\boldsymbol{x_1,\cdots,x_n}$) of the overhead line from the line sending-end to the line receiving-end to identify the critical spans during loading time $\boldsymbol{t}$. The proposed formulation in (13) meets the condition that the obtained critical line span has the longest length.

$$\mathrm{SLWOP_2^{\varphi}}: \underbrace{min}_{\forall c_{AB}\in R_c\in R_s\left(x_{seg}^{\varphi_1,\cdots,\varphi_n}\right)} \sum_{s_1}^{s_N^{\varphi}}\left\{V_{c_{AB}}^{s}\left(x_{seg}^{\varphi_1,\cdots,\varphi_n}\right)\in V_s^s\left(x_{seg}^{\varphi_1,\cdots,\varphi_n}\right)\right\} \quad (13)$$

$$\text{s.t. } \beta_{s_1,\cdots,s_N}^{x_{seg}^{\varphi_1,\cdots,\varphi_n}} > \alpha_{c_{AB}}^{x_{seg}^{\varphi_1,\cdots,\varphi_n}} \geq max\left(L_{c_{AB}}\left(x_{seg}^{\varphi_1,\cdots,\varphi_n}\right)\right)\forall R_c\in R_s\in min\left\{V_{c_{AB}}^{s}\left(x_{seg}^{\varphi_1,\cdots,\varphi_n}\right)\wedge t, V_{c_{AB}}^{s}\left(x_{seg}^{\varphi_1,\cdots,\varphi_n}\right)\vee t\right\}$$

Considering the mathematical formulation of $\mathbf{SLWOP_2^{\varphi}}$, span $\boldsymbol{c_{AB}}$ from $\boldsymbol{R_s}\left(\boldsymbol{x_{seg}^{\varphi_1,\cdots,\varphi_n}}\right)$ is an identified critical line span lying between towers $\boldsymbol{A}$ and $\boldsymbol{B}$ belonging to the set of critical spans $\boldsymbol{R_c}$ that is a subset of the total line span set $\boldsymbol{R_s}$. Further, $\mathbf{SLWOP_2^{\varphi}}$ is subject to the required sagging level, i.e., the calculated sag $\boldsymbol{\alpha}_{c_{AB}}^{x_{seg}^{\varphi_1,\cdots,\varphi_n}}$ across the identified critical span based on the DTR technique is less than the maximum allowable sag $\boldsymbol{\beta}_{s_1,\cdots,s_N}^{x_{seg}^{\varphi_1,\cdots,\varphi_n}}$ (see Section 5). To find another critical span at the next loading time $\boldsymbol{t+1}$, $\mathbf{SLWOP_2^{\varphi}}$ is updated and the procedure is continued until all critical spans are identified.

To consider solar radiation effects in identifying the critical line spans, $\mathbf{SLWOP_3^{\varphi}}$, as shown in (14), was used to determine the critical line spans facing the highest

solar radiation in the given weather conditions. The optimization problem starts by searching all line spans in (11), selecting those line spans that are the longest in length and face the highest solar radiation. The search is carried out across all $\boldsymbol{n}$ segments ($\boldsymbol{x_1, \cdots, x_n}$) of the test overhead line during loading time $\boldsymbol{t}$. The proposed formulation in (14) meets the condition that the obtained critical line span $\boldsymbol{c_{AB}}$ lying between tower $\boldsymbol{A}$ and $\boldsymbol{B}$ carries the longest length amongst all spans in the total set of line spans $\boldsymbol{R_s}\left(\boldsymbol{x_{seg}^{\varphi_1,\cdots,\varphi_n}}\right)$ experiencing the maximum solar radiation $\boldsymbol{Q_{c_{AB}}^{s}}\left(\boldsymbol{x_{seg}^{\varphi_1,\cdots,\varphi_n}}\right)$.

$$\text{SLWOP}_3^{\varphi}: \underbrace{max}_{\forall c_{AB} \in R_c \in R_s\left(x_{seg}^{\varphi_1,\cdots,\varphi_n}\right)} \sum_{s_1}^{s_N^{\varphi}} \left\{ Q_{c_{AB}}^{s}\left(x_{seg}^{\varphi_1,\cdots,\varphi_n}\right) \in Q_s^{s}\left(x_{seg}^{\varphi_1,\cdots,\varphi_n}\right) \right\} \quad (14)$$

$$\text{s.t. } \beta_{s_1,\cdots,s_N}^{x_{seg}^{\varphi_1,\cdots,\varphi_n}} > \alpha_{c_{AB}}^{x_{seg}^{\varphi_1,\cdots,\varphi_n}} \geq max\left(L_{c_{AB}}\left(x_{seg}^{\varphi_1,\cdots,\varphi_n}\right)\right) \forall R_c \in R_s \in max\left\{Q_{c_{AB}}^{s}\left(x_{seg}^{\varphi_1,\cdots,\varphi_n}\right) \wedge t, Q_{c_{AB}}^{s}\left(x_{seg}^{\varphi_1,\cdots,\varphi_n}\right) \vee t\right\}$$

Based on the mathematical formulation of $\mathbf{SLWOP_3^{\varphi}}$, span $\boldsymbol{c_{AB}}$ from $\boldsymbol{R_s}\left(\boldsymbol{x_{seg}^{\varphi_1,\cdots,\varphi_n}}\right)$ is an identified critical line span lying between towers $\boldsymbol{A}$ and $\boldsymbol{B}$ which belongs to a set of multiple critical spans $\boldsymbol{R_c}$ that further are a subset of the total line span set $\boldsymbol{R_s}$. Further, $\mathbf{SLWOP_3^{\varphi}}$ is subject to the required sagging level, i.e., the calculated sag $\boldsymbol{\alpha_{c_{AB}}^{x_{seg}^{\varphi_1,\cdots,\varphi_n}}}$ across the identified critical span based on the DTR technique is less than the maximum allowable sag $\boldsymbol{\beta_{s_1,\cdots,s_N}^{x_{seg}^{\varphi_1,\cdots,\varphi_n}}}$ (see Section 5). To find another critical line span at the next loading time $\boldsymbol{t+1}$, $\mathbf{SLWOP_3^{\varphi}}$ is updated and the procedure continues until all critical spans are identified.

To locate the critical line spans in the test overhead line, the optimization problems $\mathbf{SLWOP_1^{\varphi}}$, $\mathbf{SLWOP_2^{\varphi}}$ and $\mathbf{SLWOP_3^{\varphi}}$ need to be satisfied until all critical line spans are identified in the test line passing through multiple terrains under various weather conditions at an allowable distance from the lowest and/or mid-point of the catenary curve to the ground. The process is further demonstrated in Algorithms 2(a) and 2(b).

The proposed algorithm is based on selecting the minimum parameter value for wind speed and maximum parameter values for ambient temperature and the solar radiation in order to distinguish between critical and non-critical line spans. Similarly, in case of wind direction, the proposed algorithm requires to select either minimum or maximum value of the wind direction in order to identify the critical spans. It is important to mention that the direction of wind speed with respect to conductor axis ranges between 0° and 90°, where 0° represents true parallel wind direction to the conductor axis while 90° represents true perpendicular wind direction to the conductor axis. Due to difficulty in obtaining the real weather data regarding the wind direction across every line span under each loading interval, a fixed true perpendicular wind direction is therefore considered by the proposed algorithm and included in **SLWOP** as shown in Algorithm 2(a). The reason to consider a fixed wind blow perpendicular to the span axis instead of a fixed wind blow parallel to the span axis was derived from [21], suggesting that at low wind speeds (that is mainly the case across critical spans), true parallel wind flow along overhead lines does not occur due to natural turbulence (associated with variable wind direction) occurring at low wind speeds.

Similarly, due to unavailability of field data regarding the orientation of 517 total line spans, it is almost impossible to program the algorithm such that it selects the wind direction that will provide the least cooling across individual line spans. As the span orientation data is important in finding the actual direction of wind speed with respect to span axis, their unavailability resulted in considering a fixed wind direction with respect to each span axis providing the least conductor cooling towards critical span identification. Similarly, as mentioned in [22] due to presence of rugged terrains (mainly in New Zealand), the line direction changes extensively. The said reasons

result in the selection of fixed wind direction to obtain an optimal solution of critical span identification during each loading interval. Additionally, as mentioned in [7], wind flow along the conductor axis causes more variations in line temperature than the wind flow across the conductor axis. The crossflow wind will provide more stable location for the critical spans than the wind blowing down the axis of the conductor [7]. Therefore, another reason behind choosing a cross-flow wind direction over the concurrent wind flow was to find the stable location of critical spans during each loading time interval.

As in this paper, the primary purpose is to test the proposed algorithm on realistic simulated loading scenarios instead of validating it on actual overhead lines in the field, hence, the flow of wind direction was chosen such that it would cause least variations in line temperature and would result in stable location of critical spans across the entire subject overhead line at each loading time interval.

Likewise, it is also advantageous for transmission system operators to receive less volatile thermal line ratings at each loading time towards making the better decisions regarding the line operation and the planning. Similarly, as the chosen overhead conductor is smaller than the conductor out for maintenance, hence being a smaller conductor and carrying huge loading, it experiences large temperature variations based on small changes in load current.

Algorithm 2(a): temperature across critical spans

Input: $\left[\left[\underbrace{\left\{T^{a}_{c_{AB}}, \quad Q^{s}_{c_{AB}}\right\}}_{\substack{max \\ \forall c_{AB}\in R_c\in R_s\left(x^{\varphi_1,\cdots,\varphi_n}_{seg}\right)}}, \quad \underbrace{\left\{V^{s}_{c_{AB}}\right\}}_{\substack{min \\ \forall c_{AB}\in R_c\in R_s\left(x^{\varphi_1,\cdots,\varphi_n}_{seg}\right)}}\right] \in \left[\underbrace{\left\{L_{c_{AB}}\left(x^{\varphi_1,\cdots,\varphi_n}_{seg}\right)\right\}}_{\substack{max \\ \forall c_{AB}\in R_c\in R_s\left(x^{\varphi_1,\cdots,\varphi_n}_{seg}\right)}}\right] \in \left[\left\{\mathrm{SLWOP}^{\varphi}_{1}, \mathrm{SLWOP}^{\varphi}_{3}, \mathrm{SLWOP}^{\varphi}_{2}\right\}^{s}_{c_{AB}}\right]$

Step-1: With the help of the known weather stations data, optimal sensor placement at each segment-ends and the obtained number of spans in each line segment, the unknown

weather data across each line span is used to estimate the set of weather elements across each critical span of the test line and is given as an input to this algorithm.

$$\textbf{for} \quad \delta_{known}^{spans} = [x_k^R,\ x_{k+1}^R, x_{k+2}^R\ ]^T$$

$$R_c\left(\ x_{seg}^{\varphi_1,\cdots,\varphi_n}\right) = \left(R_s\left(\ x_{seg}^{\varphi_1,\cdots,\varphi_n}\right) - R_o\left(\ x_{seg}^{\varphi_1,\cdots,\varphi_n}\right)\right)$$

$$\delta_{unknown}^{spans} = \left[T_{c_{AB}}^a, V_{c_{AB}}^s, Q_{c_{AB}}^s\ \right]^T$$

Step 2: Due to absence of field rating data, a perpendicular direction of wind speed θ_V to the axis of critical spans is considered (based on practice as followed in [13]). The $\mathbf{SLWOP_2^{\varphi}}$ formulation is updated after wind direction consideration.

$$\textbf{for} \quad (\theta = 90°)$$

$$\left[\left\{\underbrace{\theta_{V,c_{AB}}^s}_{90°}\right\} \in \left[\underbrace{\left\{L_{c_{AB}}\left(\ x_{seg}^{\varphi_1,\cdots,\varphi_n}\ \right)\right\}}_{\substack{\underbrace{max}\\ \forall c_{AB}\in R_c\in R_s\left(\ x_{seg}^{\varphi_1,\cdots,\varphi_n}\right)}}\right]\right] \ni \left[\{\mathrm{SLWOP}_2^{\varphi}\}_{c_{AB}}^s\right]$$

Step 3: The resulting ambient-span length data from step 1, the critical span formulations from $\mathbf{SLWOP_1^{\varphi}}$, $\mathbf{SLWOP_2^{\varphi}}$ and $\mathbf{SLWOP_3^{\varphi}}$,wind direction (normal to span axis)-span length data from step 2, and the line's physical dimensions were used as input to line rating techniques to find the line temperature across the identified critical spans in each segment of the test line and thus obtain the temperature across the most critical span of the line at time $\boldsymbol{t}$ and at subsequent timings, i.e., in case of DTR,

$$\textbf{for} \quad T_{DTR,c_{AB}}\left(\ x_{seg}^{\varphi_1,\cdots,\varphi_n}\ \right) \leftarrow \left[\left(max\sum_{\varphi=1}^{n} I_{max}^{\varphi}\right) \ni Input\right]$$

$$T_{DTR,c_{AB}}\left(\ x_{seg}^{\varphi_1,\cdots,\varphi_n}\ \right) = max\left[T_{DTR,c_{AB}}\left(\ x_{seg}^{\varphi_1}\ \right),\cdots,T_{DTR,c_{AB}}\left(\ x_{seg}^{\varphi_n}\ \right)\right]$$

where, the maximum line current $\boldsymbol{I_{max}}$ (based on Scenarios A & B) found at the MAT limit at loading time $\boldsymbol{t}$ and the subsequent loading times in the presence of real weather conditions were passed through each critical span in all line segments $\boldsymbol{x_{seg}^{\varphi_1,\cdots,\varphi_n}}$ to obtain the maximum critical span temperature using the DTR technique $\boldsymbol{T_{DTR}}$. Similarly, in the case of STR, $\boldsymbol{I_{max}}$ found at MAT limit at loading time $\boldsymbol{t}$ and the subsequent loading times in presence of assumed-weather conditions were passed through each critical span in all line segments

$x_{seg}^{\varphi_1,\cdots,\varphi_n}$ to obtain the maximum critical span temperature under the STR technique T_{STR}, i.e.,

$$\textbf{for} \quad T_{STR,c_{AB}}\left(x_{seg}^{\varphi_1,\cdots,\varphi_n}\right) \leftarrow \left[\left(max\sum_{\varphi=1}^{n} I_{max}^{\varphi}\right) \ni Input\right]$$

$$T_{STR,c_{AB}}\left(x_{seg}^{\varphi_1,\cdots,\varphi_n}\right) = max\left[T_{STR,c_{AB}}\left(x_{seg}^{\varphi_1}\right),\cdots,T_{STR,c_{AB}}\left(x_{seg}^{\varphi_n}\right)\right]$$

where, T_{STR} was found after assuming the worst weather across each span of the test line. The resulting critical span-based temperature was thereafter used as the maximum temperature of the entire line during that time and line loading, and then for subsequent loading time intervals.

$$\left|T_{DTR,c_{AB}}\left(x_{seg}^{\varphi_1,\cdots,\varphi_n}\right)\right| \leq T_{MAT}\left(x_{seg}^{\varphi_1,\cdots,\varphi_n}\right) \leq T_{STR,c_{AB}}\left(x_{seg}^{\varphi_1,\cdots,\varphi_n}\right)$$

end

Output: $\left[T_{DTR,c_{AB}}\left(x_{seg}^{\varphi_1,\cdots,\varphi_n}\right), T_{STR,c_{AB}}\left(x_{seg}^{\varphi_1,\cdots,\varphi_n}\right)\right]$

Algorithm 2(b): sag across critical spans

Input: $\left[T_{DTR,c_{AB}}\left(x_{seg}^{\varphi_1,\cdots,\varphi_n}\right), T_{STR,c_{AB}}\left(x_{seg}^{\varphi_1,\cdots,\varphi_n}\right)\right]$

Step 1: The critical span-temperature from Algorithm-2(a) with span-topography and physical dimensions under both line rating techniques is used as an input to the line sag modelling to result in sagging across the critical spans. Due to dynamic weather conditions, the sag across critical line spans in presence of the actual weather (Sag_{DTR}) is lower than the sag under the worst weather (Sag_{STR}).

$$\textbf{for} \quad Sag_{DTR,c_{AB}}\left(x_{seg}^{\varphi_1,\cdots,\varphi_n}\right) \leftarrow T_{DTR,c_{AB}}\left(x_{seg}^{\varphi_1,\cdots,\varphi_n}\right)$$

$$Sag_{STR,c_{AB}}\left(x_{seg}^{\varphi_1,\cdots,\varphi_n}\right) \leftarrow T_{STR,c_{AB}}\left(x_{seg}^{\varphi_1,\cdots,\varphi_n}\right)$$

$$\underbrace{Sag_{STR,c_{AB}}}_{\beta_{s_1,\cdots,s_N}^{x_{seg}^{\varphi_1,\cdots,\varphi_n}} > \alpha_{c_{AB}}^{x_{seg}^{\varphi_1,\cdots,\varphi_n}}} > \underbrace{Sag_{DTR,c_{AB}}}_{\beta_{s_1,\cdots,s_N}^{x_{seg}^{\varphi_1,\cdots,\varphi_n}} > \alpha_{c_{AB}}^{x_{seg}^{\varphi_1,\cdots,\varphi_n}}}$$

end

Output: $\left[Sag_{DTR,c_{AB}}\left(x_{seg}^{\varphi_1,\cdots,\varphi_n}\right), Sag_{STR,c_{AB}}\left(x_{seg}^{\varphi_1,\cdots,\varphi_n}\right)\right]$

Step 4) Sag Modelling

The last step of the proposed technique is sag modelling of the identified critical line spans under static and dynamic weather conditions as shown in Algorithm 2(b). This study considered sagging across spans passing through both flat and non-flat terrains to better represent the change in movement of the lowest point(s) across the test overhead line. As obtained from the results (see Section 5), this movement in the lowest point (s) across the conductor changes from mid-span (in flat spans) to the lower suspension point (in non-flat spans).

Span sagging was obtained by inputting the static and dynamic ampacity-based span temperature and the span lengths in (1)-(7) from [23] during both static and dynamic weather conditions under both scenarios. In addition to weather and loading conditions, span length is also an important factor in causing span sagging [23, 24] and is therefore considered in SLWOP. Based on the obtained results, spans of smaller lengths facing the worst weather were found to exhibit minimum sagging even at loading temperatures above the MAT limit; hence such spans, despite facing conductor temperatures above the safe allowable limit, were still categorized as non-critical line spans because of the clearance margin available. Therefore, it can be concluded that span-length is an important factor in determining span sagging, in addition to weather conditions, and thus cannot be neglected when identifying critical line spans. This important factor is however ignored in the critical-span identification techniques proposed in [5]-[8].

3.2. Proposed versus conventional algorithm implementation overview

The conventional critical span identification technique as discussed in this paper starts by back-calculating the temperature across each line span through ampacity and weather conditions surrounding individual spans in the entire test overhead line.

On the other hand, the proposed technique in this paper under SLWOP methodology searches each line span to identify the spans with longest length and worst ambient conditions, further represented as critical spans. After initial critical span identification, the proposed technique calculates their temperature and the sagging-levels by allowing the maximum allowable current (ampacity) through the test overhead line. The spans with minimum thermal loadability are identified as critical spans and validated using the conventional technique. The procedure to find the sagging across critical (proposed technique) and all line spans (conventional technique) is illustrated in the flow chart as shown in Fig. 5.

The convergence of proposed technique to identify critical spans from all line spans took at average ~10 times lower computational time than the conventional technique for the same overhead line when executed in Intel Core i7-8700 CPU@3.2 GHz, 32.0 GB RAM system under a single scenario condition from t= 20 min to t= 25 min. The proposed technique can therefore be considered as reliable, fast, efficient and computationally inexpensive in identifying critical spans in a large overhead line passing through multiple terrains traversing varied geographical regions.

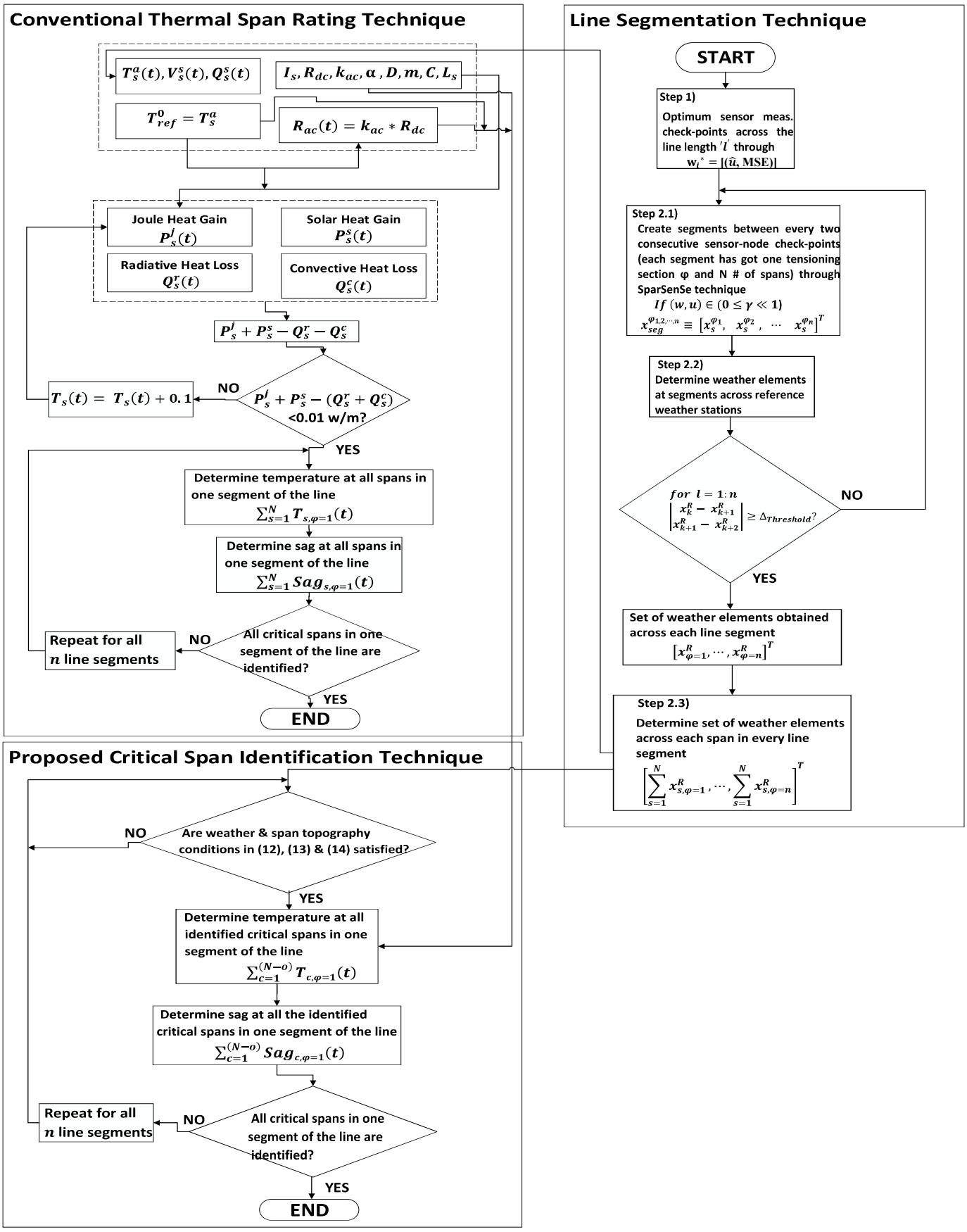

Fig. 5 Critical span identification through proposed and conventional algorithms

4. Case study

4.1. Background

To find the maximum thermal capacity, the test line was loaded under multiple time- and space-dependent weather conditions until it reached the maximum safe thermal limit. The applied loading conditions in the following scenarios determined the line's ability to relieve congestion with no ground clearance infringement. The 10-min interval based ambient variables on a hottest day in January-2019 were taken from the weather stations as shown in Table 3 along the route of the test overhead line. The typical day selection was based on obtaining the less favourable weather conditions to find critical spans and their influence to limiting the line DTR.

Two case scenarios are carried out in this study to analyse the capacity of the test line to overcome possible congestion. The resulting congestion may jeopardise the system reliability if the test line is not provided with reliable ambient data across each span regardless of their orientation and location. The retrieval of weather data across each line span will enable the possibility of applying the DTR technique such that the line delivers optimum electricity at maximum potential and at no risk of thermal and voltage violations. This study helps in individual monitoring of span weather conditions to better estimate the ambient variable distribution across the entire route of the test line toward reliable line flow.

4.2. Scenario-A——Line outage

This scenario presents the N-1 contingency state in result of the Line-2 shutdown, making the test line to dispatch excess electricity. Following the N-1 contingency, the resulting line load may increase congestion across the test line mainly due to presence of line hot spots and due to their possible remote location from the weather stations toward receiving the reliable ambient data at each loading.

The obtained results further indicate that the test line under DTR technique is capable to overcome the subsequent loading in comparison to the STR technique. Under this case scenario, the test line is investigated through static and dynamic weather conditions in the presence of a 550 MW base load from t=0 min to t= 30 min. At t=10 min, the adjacent overhead line on the same tower was disconnected (simulating the need to carry out maintenance work) for 10 min and was thus restored at t=20 min. DTR-and static thermal rating (STR)-based conductor temperatures for critical spans in this scenario are shown in Table 4.

Table 4 Critical spans temperature under Scenario——A

Time (min.)	**Line-1 Current (A)**	**Critical Span-1 Temperature (°C)**		**Critical Span-2 Temperature (°C)**		**Critical Span-3 Temperature (°C)**	
		DTR	**STR**	**DTR**	**STR**	**DTR**	**STR**
0	405	40.33	61.92	40.38	61.92	40.42	61.92
5	405	40.96	61.92	41.34	61.92	41.26	61.92
10	536	54.26	84.48	54.97	84.48	54.84	84.48
15	536	53.34	84.48	54.35	84.48	54.71	84.48
20	536	53.80	84.48	53.66	84.48	54.37	84.48
25	405	43.53	70.56	43.48	70.56	43.25	70.56
30	405	41.13	61.92	41.18	61.92	40.29	61.92

4.3. Scenario-B—— Emergency overloading

The test overhead line in Scenario-B was examined under elevated time-domain load conditions. From t=0 min to t= 5 min, line loading was investigated under static and dynamic weather conditions in the presence of critical spans under a 550 MW base load, resulting in critical span temperatures as shown in Table 5. At t=5 min, the base load was increased 1.3 p.u. At t=10 min, an additional increment to 1.5 p.u. was carried out, further continued to 1.8 p.u. at t=15 min and 2.0 p.u. at t=20 min. At

t= 25 min, the adjacent line on the same tower in the double AC circuit was restored while the test line was under twice the base load. At t=30 min, 0.2 p.u. load decrement was undertaken across the test overhead line. The obtained results as shown in Table 5 indicate that, at t=20 min, when the test line experienced the worst loading combined with the worst weather, the DTR-based temperature across all critical spans was found slightly above the MAT limit of the test line, i.e., across critical span-1, it was found to 1.26% above, across critical span-2 and critical apsn-3 was found 1.08% and 1.67% respectively. The STR based temperature across all identified critical line spans was found above the MAT limit from t=0 min to t=25 min due to excess demand from the load side.

Table 5 Critical spans temperature under Scenario——B

Time (min.)	Line-1 Current (A)	Critical Span-1 Temperature (°C)		Critical Span-2 Temperature (°C)		Critical Span-3 Temperature (°C)	
		DTR	STR	DTR	STR	DTR	STR
0	536	50.52	84.48	50.55	84.48	50.54	84.48
5	596	57.31	84.48	57.68	84.48	57.57	84.48
10	636	65.49	84.48	66.24	84.48	66.10	84.48
15	696	72.45	84.48	73.40	84.48	73.59	84.48
20	737	81.01	84.48	80.87	84.48	81.34	84.48
25	553	58.77	84.48	58.72	84.48	58.50	84.48
30	479	47.77	70.53	47.81	70.53	46.92	70.53

5. Results

The conventional critical span identification technique starts by back-calculating the line temperature across each span through ampacity and surrounding weather conditions for each line span as shown in Fig. 5. The proposed technique under SLWOP methodology, as shown in Fig. 5 searches each line span to identify the spans with longest length and worst ambient conditions, further represented as

critical line spans in the test line. The design technique thereafter calculates the temperature and sagging across the identified critical spans by allowing the maximum allowable current (ampacity). The spans with the highest levels of sagging were then identified as critical spans and validated using the conventional technique. The line temperature across each span was used to find the individual span sagging.

5.1. Conventional technique based critical span sagging

When implemented from t=20 min to t=25 min under the worst loading conditions in Scenario-B, the conventional technique resulted in three critical span identifications at 42.92 km, 48.34 km and 55.64 km from the line sending-end, as shown in Fig. 6.

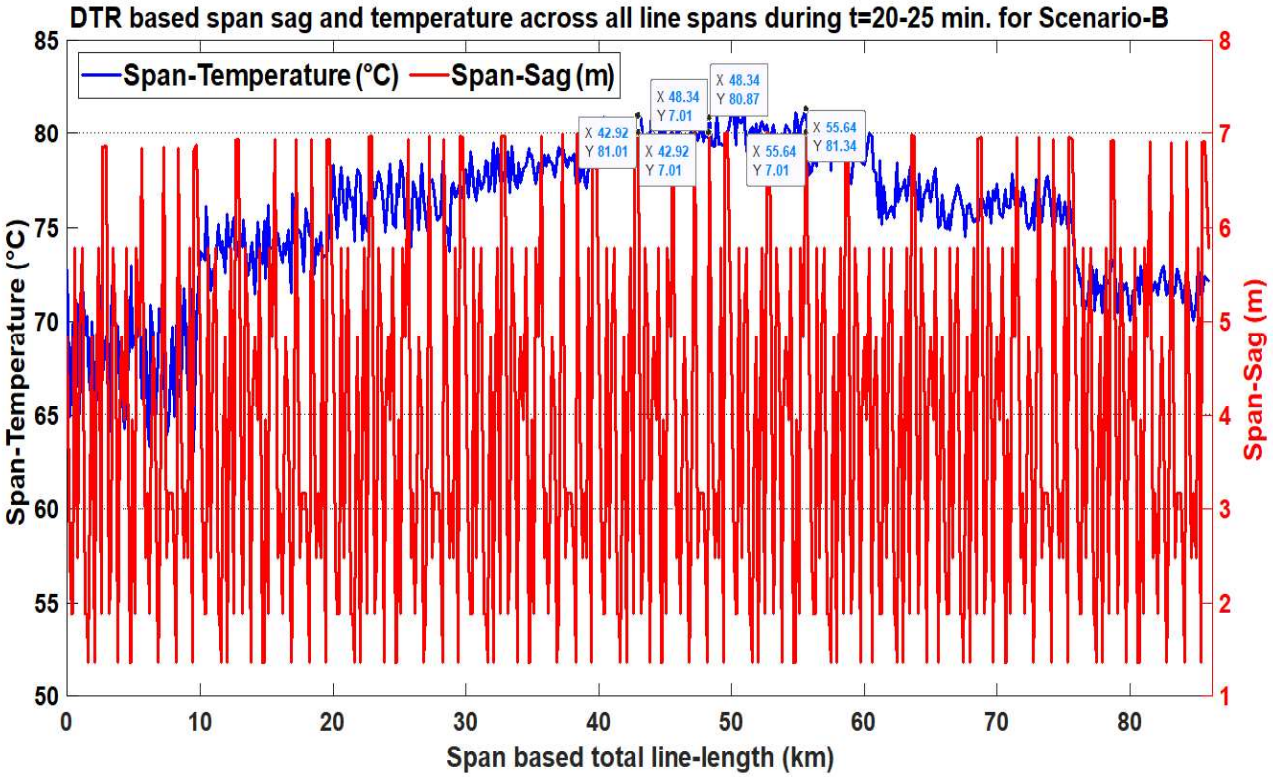

Fig. 6 Critical spans identification through conventional technique

5.2. *Proposed technique based critical span sag-temperature validation*

Based on results as shown in Fig. 7, the proof of concept of the proposed algorithm is validated. The results were obtained under worst loading conditions from

t=20 min to t=25 min across the test line with all identified critical line spans passing through flat terrains. The results indicate that the proposed algorithm resulted in the same set of critical spans at the same locations as obtained under the conventional technique.

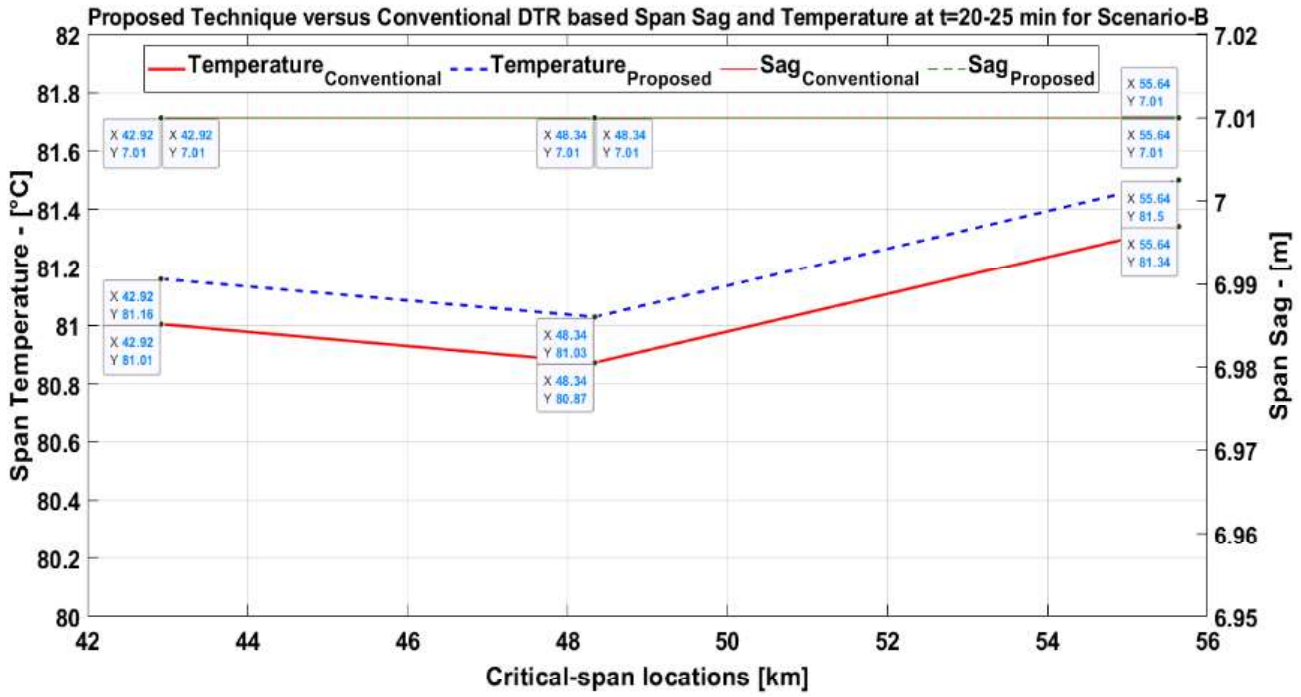

Fig. 7 Sag and temperature across all critical line spans passing through flat terrains based on conventional and proposed techniques under Scenario-B from t= 20 min to t= 25 min

To further validate the proposed technique, it was applied for all other temporal loadings, with and without space- and time-dependent weather conditions from t= 0 min to t= 30 min under both scenarios, resulting in critical span temperatures and their respective sagging levels as shown in Table 6 when passing through flat terrains and in Table 7 when passing through non-flat terrains. The results in Table 6 and Table 7 further indicate that critical span-1, when passing through non-flat terrain, experienced on average 2.88% more sag under the DTR technique than when passing through flat terrain subject to the same loading and weather.

Table 6 Sag across critical spans passing through flat terrains

Time (min)	Scenario-A						Scenario-B					
	Critical Span-1		Critical Span-2		Critical Span-3		Critical Span-1		Critical Span-2		Critical Span-3	
	DTR	STR	DTR	STR	DTR	STR	DTR	STR	DTR	STR	DTR	STR
	Sag (m)	Sag (m)	Sag (m)	Sag (m)	Sag (m)	Sag (m)	Sag (m)	Sag (m)	Sag (m)	Sag (m)	Sag (m)	Sag (m)
0	6.56	6.79	6.56	6.79	6.56	6.79	6.67	7.05	6.67	7.05	6.67	7.05
5	6.56	6.79	6.57	6.79	6.57	6.79	6.76	7.05	6.76	7.05	6.76	7.05
10	6.71	7.05	6.72	7.05	6.71	7.05	6.85	7.05	6.85	7.05	6.85	7.05
15	6.70	7.05	6.71	7.05	6.71	7.05	6.93	7.05	6.95	7.05	6.95	7.05
20	6.70	7.05	6.70	7.05	6.71	7.05	7.01	7.05	7.01	7.05	7.01	7.05
25	6.59	6.89	6.59	6.89	6.59	6.89	6.76	7.05	6.76	7.05	6.75	7.05
30	6.57	6.79	6.57	6.79	6.56	6.79	6.64	6.89	6.64	6.89	6.63	6.89

Table 7 Sag across critical spans passing through non-flat terrains

Time (min)	Scenario-A						Scenario-B					
	Critical Span-1		Critical Span-2		Critical Span-3		Critical Span-1		Critical Span-2		Critical Span-3	
	DTR	STR	DTR	STR	DTR	STR	DTR	STR	DTR	STR	DTR	STR
	Sag (m)	Sag (m)	Sag (m)	Sag (m)	Sag (m)	Sag (m)	Sag (m)	Sag (m)	Sag (m)	Sag (m)	Sag (m)	Sag (m)
0	6.75	6.99	6.75	6.99	6.75	6.99	6.86	7.25	6.86	7.25	6.86	7.25
5	6.75	6.99	6.76	6.99	6.76	6.99	6.95	7.25	6.96	7.25	6.96	7.25
10	6.90	7.25	6.91	7.25	6.91	7.25	7.05	7.25	7.05	7.25	7.05	7.25
15	6.89	7.25	6.90	7.25	6.91	7.25	7.14	7.25	7.15	7.25	7.15	7.25
20	6.90	7.25	6.90	7.25	6.90	7.25	7.21	7.25	7.21	7.25	7.22	7.25
25	6.78	7.09	6.78	7.09	6.78	7.09	6.95	7.25	6.95	7.25	6.95	7.25
30	6.76	6.99	6.76	6.99	6.75	6.99	6.83	7.09	6.83	7.09	6.82	7.09

Similarly, critical span-2, when passing through non-flat terrain, experienced on average 2.88% more sag under the DTR technique than when passing through flat terrain under the same weather and loading conditions. In case of critical span-3, when passing through non-flat terrain it experienced on average 2.91% more sag under the DTR technique than when passing through flat terrain under identical weather and loading conditions. Figs. 8-9 illustrate vertical sag across critical span-3 of the test line under DTR technique from t= 20 min to t= 25 min when passing through flat and non-flat terrains, respectively, under Scenario-B.

Besides sag, the vertical distance of each line span to the ground is also important for transmission system operators to carry out a reliable line loading. Due to unavailability of under span terrain topography data for each line span before and after the line loading, the actual vertical clearance across critical spans was not found and is left as a future work subject to availability of the field data pertaining to span terrain topography. As a future work, the actual minimum vertical distance to ground will be considered across every line span to validate the proposed algorithm on real line loading.

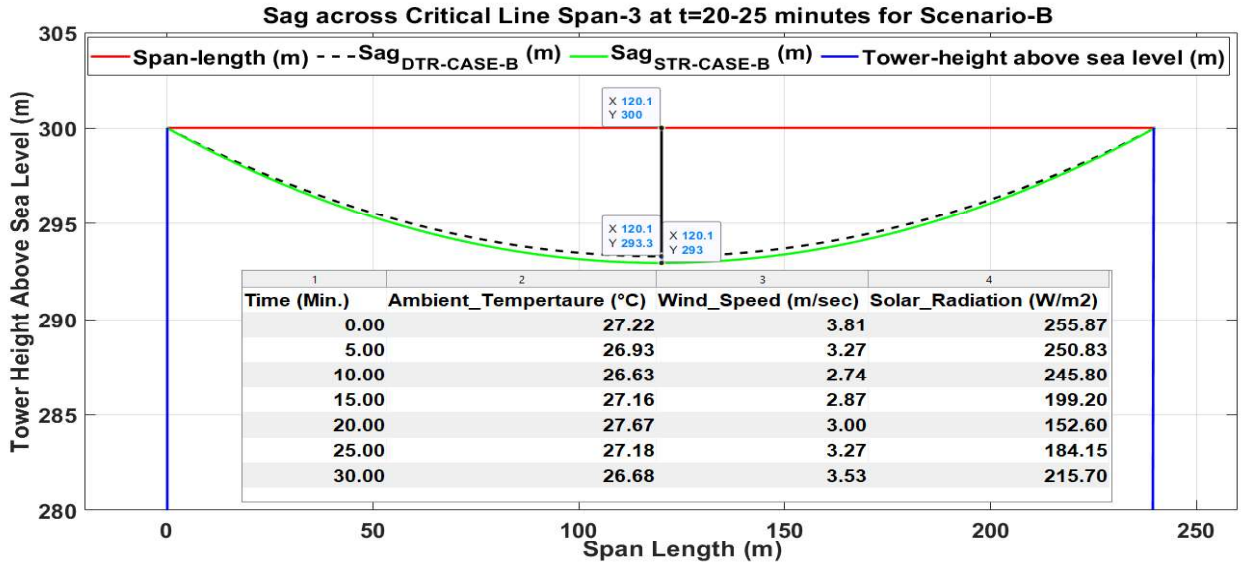

Time (Min.)	Ambient_Tempertaure (°C)	Wind_Speed (m/sec)	Solar_Radiation (W/m2)
0.00	27.22	3.81	255.87
5.00	26.93	3.27	250.83
10.00	26.63	2.74	245.80
15.00	27.16	2.87	199.20
20.00	27.67	3.00	152.60
25.00	27.18	3.27	184.15
30.00	26.68	3.53	215.70

Fig. 8 Critical span-3 sagging when passing through flat terrain under t=20- 25 min

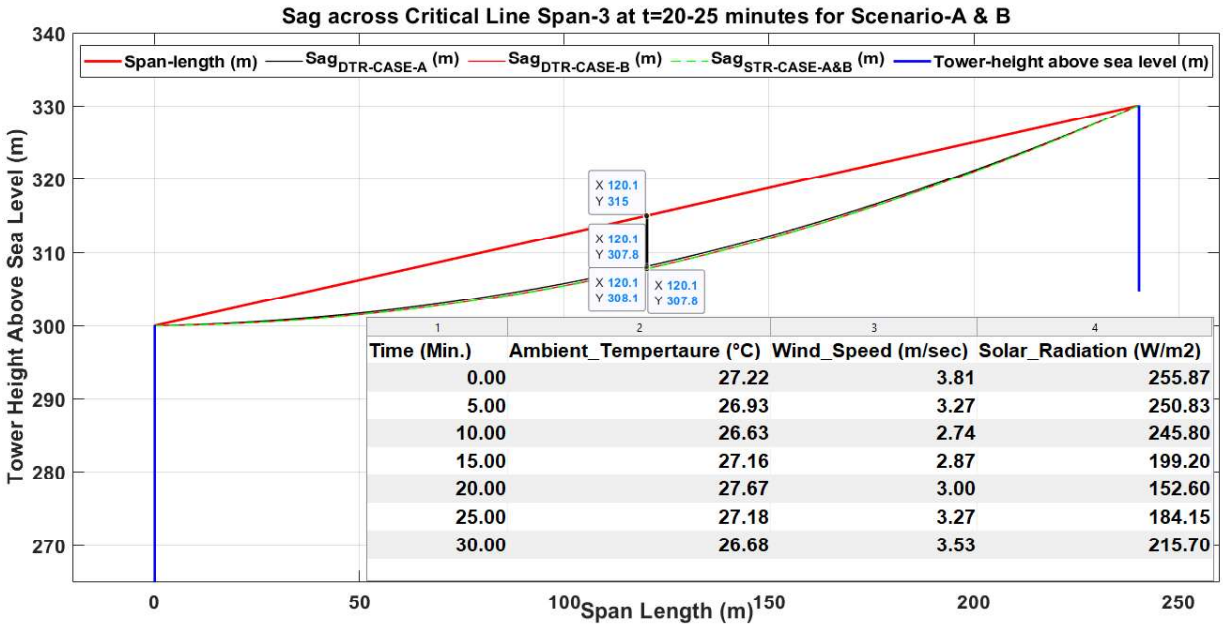

Time (Min.)	Ambient_Tempertaure (°C)	Wind_Speed (m/sec)	Solar_Radiation (W/m2)
0.00	27.22	3.81	255.87
5.00	26.93	3.27	250.83
10.00	26.63	2.74	245.80
15.00	27.16	2.87	199.20
20.00	27.67	3.00	152.60
25.00	27.18	3.27	184.15
30.00	26.68	3.53	215.70

Fig. 9 Critical span-3 sagging when passing through non-flat terrain under t=20-25 min

6. Conclusion

This paper presents a novel technique to identify the critical spans across an overhead line operating under the DTR technique at the least computational cost. Optimal sensor placement used reference weather stations to determine the unknown weather elements across each span of the test line. The technique produced non-uniform segments, which contained multiple critical and non-critical spans. Using the proposed critical-span identification technique, critical spans were identified based on weather and span-topography conditions.

The resulting critical spans were used to determine the thermal rating for the entire test line under static and real weather conditions. These spans were observed to have high sagging levels because they faced the worst weather and had the longest span lengths. These factors determined the global minimum of the line DTR to avoid ground clearance infringement across any line span, and thus control line loadability within allowable sag limits.

To validate the accuracy and computational efficiency of the proposed technique against the conventional technique, critical span identification using the conventional technique was carried out by computing the DTR across each span of the test overhead line, based on specified loadings and real weather conditions, to obtain the temperature and sag across each line span. The spans with the greatest sag were those with the highest conductor temperature and the longest span-length at the threshold of the MAT limit and were therefore identified as critical spans by the conventional technique.

The critical spans identified using the conventional technique were identical to those identified by the proposed technique. In the proposed technique, line temperature and sag across each individual span are not calculated; rather, the technique identifies spans as critical based on their surrounding weather conditions, topography and length. Based on the results obtained, the proposed technique is reliable and computationally cost-effective, and effective in differentiating critical and non-critical line spans across a non-uniformly segmented overhead line.

7. References

[1] "Oncor's pioneering transmission dynamic line rating (DLR) demonstration lays foundation for follow-on deployments," U.S. Dept. Energy, MD, USA, 2014.

[2] Final Report of Oncor-DOE Smart Grid Development Project fully documenting the DOE supported DLR project. [Online]. Available: https://www.smartgrid.gov/files/FTR_Final_Oncor_DE-OE0000320.pdf. Accessed on 5th November 2019.

[3] V. Cecchi, M. Knudson and K. Miu, "System Impacts of Temperature-Dependent Transmission Line Models," in *IEEE Transactions on Power Delivery*, vol. 28, no. 4, pp. 2300-2308, Oct. 2013. doi: 10.1109/TPWRD.2013.2276757.

[4] V. Cecchi, A. S. Leger, K. Miu and C. O. Nwankpa, "Incorporating Temperature Variations Into Transmission-Line Models," in *IEEE Transactions on Power*

Delivery, vol. 26, no. 4, pp. 2189-2196, Oct. 2011. doi: 10.1109/TPWRD.2011.2159520.

[5] J. Teh and I. Cotton, "Critical span identification model for dynamic thermal rating system placement," in *IET Generation, Transmission & Distribution*, vol. 9, no. 16, pp. 2644-2652, 3 12 2015. doi: 10.1049/iet-gtd.2015.0601.

[6] M. Matus *et al*., "Identification of Critical Spans for Monitoring Systems in Dynamic Thermal Rating," in *IEEE Transactions on Power Delivery*, vol. 27, no. 2, pp. 1002-1009, April 2012. doi: 10.1109/TPWRD.2012.2185254.

[7] J. W. Jerrell, W. Z. Black and T. J. Parker, "Critical span analysis of overhead conductors," in *IEEE Transactions on Power Delivery*, vol. 3, no. 4, pp. 1942-1950, Oct. 1988. doi: 10.1109/61.194004.

[8] J. Wan *et al*., "Determination of critical span in real time using proper orthogonal decomposition," *2013 Seventh International Conference on Sensing Technology (ICST)*, Wellington, 2013, pp. 816-821. doi: 10.1109/ICSensT.2013.6727765.

[9] A. Hatibovics, "Determination of the lowest point of the conductor in inclined spans based on a known maximal sag of the parabola," *22nd International Conference and Exhibition on Electricity Distribution (CIRED 2013)*, Stockholm, 2013, pp. 1-4. doi: 10.1049/cp.2013.0583.

[10] Talpur, Saifal, T. T. Lie, and R. Zamora. "Non-steady state electro-thermally coupled weather-dependent power flow technique for a geographically-traversed overhead-line capacity improvement." Electric Power Systems Research 177 (2019): 106017. doi: 10.1016/j.epsr.2019.106017.

[11] IEEE Standard for Calculating the Current-Temperature Relationship of Bare Overhead Conductors," in IEEE Std 738-2012 (Revision of IEEE Std 738-2006 - Incorporates IEEE Std 738-2012 Cor 1-2013), vol., no., pp.1-72, 23 Dec. 2013. doi: 10.1109/IEEESTD.2013.6692858.

[12] Deb, Anjan K. Powerline ampacity system: theory, modeling and applications. CRC Press, 2017.

[13] Morgan, Vincent T. "The thermal behaviour of electrical conductors." (Research Studies Press, 1997).

[14] Ausgrid (2015) Network standard NS220. “Overhead design manual, NW000-S0092.” Ausgrid.

[15] National Institute of Water and Atmospheric Research (NIWA). [Online]. Available: https://cliflo.niwa.co.nz/. Accessed on 31st May 2019.

[16] Küchenhoff, Helmut. "An exact algorithm for estimating breakpoints in segmented generalized linear models." (1996).

[17] H. Jamali-Rad, A. Simonetto and G. Leus, "Sparsity-Aware Sensor Selection: Centralized and Distributed Algorithms," in IEEE Signal Processing Letters, vol. 21, no. 2, pp. 217-220, Feb. 2014. doi: 10.1109/LSP.2013.2297419.

[18] C. Jiang, Y. C. Soh and H. Li, "Sensor Placement by Maximal Projection on Minimum Eigenspace for Linear Inverse Problems," in IEEE Transactions on Signal Processing, vol. 64, no. 21, pp. 5595-5610, 1 Nov.1, 2016. doi: 10.1109/TSP.2016.2573767.

[19] Grant, Michael, Stephen Boyd, and Yinyu Ye. "CVX: Matlab software for disciplined convex programming (2008)." Web page and software available at http://stanford. edu/~ boyd/cvx (2015).

[20] Ryan, Sandra E., and Laurie S. Porth. "A tutorial on the piecewise regression approach applied to bedload transport data." Gen. Tech. Rep. RMRS-GTR-189. Fort Collins, CO: US Department of Agriculture, Forest Service, Rocky Mountain Research Station. 41 p. 189 (2007).

[21] Morgan, V. T. "The current-carrying capacities of overhead-line conductors." (1978).

[22] Dino, A., A. Ketley, and G. McDougall. "Dynamic transmission line rating: Technology review." Hydro Tasmania Consulting 30 (2009).

[23] C. O. Boyse and N. G. Simpson, "The problem of conductor sagging on overhead transmission lines," in Journal of the Institution of Electrical Engineers - Part II: Power Engineering, vol. 91, no. 21, pp. 219-238, June 1944. doi: 10.1049/ji-2.1944.0029.

[24] Muhr, Michael, et al. "Calculation of overhead line sags." 51st Internationales Wissenschaftliches Kolloquium. Vol. 10. 2006.

***Declaration of Interest Statement**

Declaration of interests

☒ The authors declare that they have no known competing financial interests or personal relationships that could have appeared to influence the work reported in this paper.

☐The authors declare the following financial interests/personal relationships which may be considered as potential competing interests: